BIOCHEMISTRY
including biophysical chemistry & molecular biology

Article

pubs.acs.org/biochemistry

An Outer Membrane Protein Undergoes Enthalpy- and Entropy-Driven Transitions

Belete R. Cheneke,[†] Mridhu Indic,[‡] Bert van den Berg,[‡] and Liviu Movileanu*[,†,§]

[†]Department of Physics, Syracuse University, 201 Physics Building, Syracuse, New York 13244-1130, United States
[‡]Program in Molecular Medicine, University of Massachusetts Medical School, Worcester, Massachusetts 01605, United States
[§]Syracuse Biomaterials Institute, Syracuse University, 121 Link Hall, Syracuse, New York 13244, United States

Supporting Information

ABSTRACT: β-Barrel membrane proteins often fluctuate among various open substates, yet the nature of these transitions is not fully understood. Using temperature-dependent, single-molecule electrophysiology analysis, along with rational protein design, we show that OccK1, a member of the outer membrane carboxylate channel from *Pseudomonas aeruginosa*, features a discrete gating dynamics comprising both enthalpy-driven and entropy-driven current transitions. OccK1 was chosen for the analysis of these transitions, because it is a monomeric transmembrane β-barrel of a known high-resolution crystal structure and displays three distinguishable, time-resolvable open substates. Native and loop-deletion OccK1 proteins showed substantial changes in the activation enthalpies and entropies of the channel transitions, but modest alterations in the equilibrium free energies, confirming that the system never departs from equilibrium. Moreover, some current fluctuations of OccK1 indicated a counterintuitive, negative activation enthalpy, which was compensated by a significant decrease in the activation entropy. Temperature scanning of the single-channel properties of OccK1 exhibited a thermally induced switch of the energetically most favorable open substate at the lowest examined temperature of 4 °C. Therefore, such a semiquantitative assessment of the current fluctuation dynamics not only demonstrates the complexity of channel gating but also reveals distinct functional traits of a β-barrel outer membrane protein under different temperature circumstances.

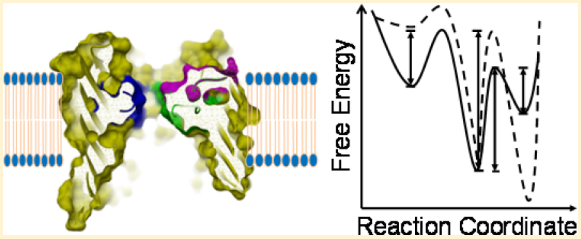

It is thought that a β-barrel structure is quite rigid, because of the network of backbone hydrogen bonds among the neighboring antiparallel β-strands.[1] Spontaneous, thermally induced current fluctuations are often observed in β-barrel outer membrane proteins.[2,3] Two major mechanisms were proposed for the gating of β-barrel membrane protein channels: (i) the electrostatic mechanism, which involves local electrostatic forces within the constriction of the protein channel, thus precluding the ions from traversing the limiting barrier,[4,5] and (ii) the steric mechanism, which implies stochastic movements of long extracellular loops folded back into the channel lumen.[6,7] Gating of β-barrel proteins has been studied extensively using various methodologies, such as single-channel electrical recordings,[8,9] rational membrane protein design,[6,7,10,11] atomic force microscopy,[12] nuclear magnetic resonance (NMR) spectroscopy,[13] X-ray crystallography,[14] and molecular dynamics simulations.[15,16] Despite significant progress in identifying the mechanisms responsible for discrete fluctuation dynamics,[12,17] we do not have a detailed quantitative understanding of the kinetics and energetics of the thermally activated current fluctuations in a β-barrel protein channel.

Recently, we explored the gating of the OccK1 protein and found that it exhibits three well-defined open substates.[18] OccK1, which was previously named OpdK,[19] is an archetype of the outer membrane carboxylate channel K (OccK) subfamily from *Pseudomonas aeruginosa*.[20−23] The X-ray crystal structure of OccK1 reveals a monomeric, 18-stranded β-barrel with a kidney-shaped central pore (Figure 1).[22,24] The channel lumen includes long extracellular loops L3, L4, and L7 and features a 5 Å diameter central constriction. Our hypothesis was that the presence of large extracellular loops L3, L4, and L7 within the channel lumen impacts the nature of the current fluctuations of the OccK1 protein (Supporting Information, Table S1). Thus, we relied upon the recently determined high-resolution X-ray crystal structure of this outer membrane protein (Figure 1).[22]

Here, the discrete gating dynamics of OccK1 reveals both enthalpy- and entropy-driven current fluctuations. We employed single-channel, temperature-dependent electrical recordings and loop-deletion protein design (Supporting Information) to explore alterations in the kinetics and energetics of the discrete current fluctuations of the OccK1 protein. A semiquantitative Arrhenius-based approach was implemented to obtain activation enthalpies as well as equilibrium free energies, enthalpies, and entropies for all current fluctuations. Loop-deletion OccK1 derivatives employing loops L3 and L4, each of which lacks an intramolecular salt bridge and several hydrogen bonds, showed significant

Received: March 11, 2012
Revised: June 5, 2012
Published: June 8, 2012

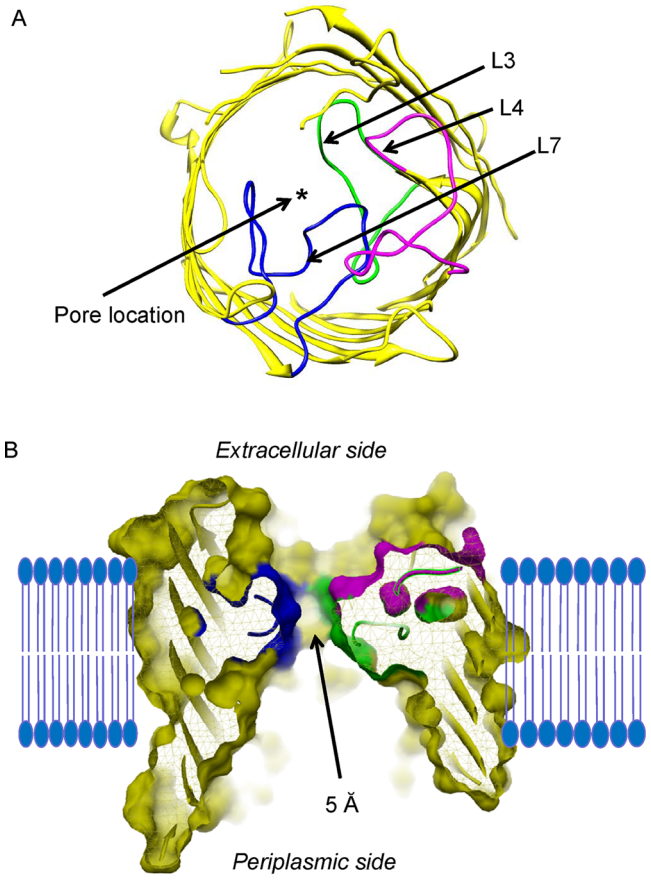

Figure 1. Structure of the wild-type OccK1 protein (WT-OccK1).[24] (A) Cross-sectional view of the WT-OccK1 protein from the extracellular side. The location of the pore constriction is shown with an asterisk. (B) Cross-sectional view along the axis of the pore lumen of the WT-OccK1 protein inserted into a planar lipid bilayer. Regions colored green, magenta, and blue indicate the positions of major extracellular loops L3, L4, and L7, respectively.

modifications in the transition and equilibrium enthalpies, but modest changes in the equilibrium free energies.

MATERIALS AND METHODS

Cloning, Overexpression, and Purification of the OccK1 Protein and Loop-Deletion OccK1 Mutants. The *occk1* gene lacking the part encoding the signal sequence was amplified from genomic DNA of *P. aeruginosa* and was then cloned into the pB22 vector[25] with the *Escherichia coli YtfM* signal sequence at the N-terminus. We also introduced a seven-His tag at the N-terminus and a TEV protease cleavage site for the removal of the His tag. The ΔL3, ΔL4, and ΔL7 loop deletions of the OccK1 protein were made by polymerase chain reaction (Expand high fidelity PCR system, Roche) (Supporting Information, Table S2). The proteins were expressed in *E. coli* C43(DE3) cells and purified by His tag chromatography. Other details of the standard protein chemistry protocols used in this work were published previously.[18] The purity of the OccK1 protein samples was assessed by sodium dodecyl sulfate−polyacrylamide gel electrophoresis (SDS−PAGE) (Supporting Information, Figure S2). Expression and purification of the loop-deletion OccK1 mutants were conducted in the same way as for the WT-OccK1 protein.

Single-Channel Current Recordings on Planar Lipid Bilayers. Single-channel current measurements were performed with planar lipid membranes.[26] The electrolyte in both chambers consisted of 2000 mM KCl and 10 mM potassium phosphate (pH 7.4), unless otherwise stated. The bilayer was formed with 1,2-diphytanoyl-*sn*-glycerophosphocholine (Avanti Polar Lipids Inc., Alabaster, AL). OccK1 was added to the *cis* chamber, which was at ground. Current flow shown as positive represents a positive charge moving from the *trans* chamber to the *cis* chamber. Currents were recorded by using an Axopatch 200B patch-clamp amplifier (Axon Instruments, Foster City, CA) connected to the chambers by Ag/AgCl electrodes.[7] The single-channel electrical traces were filtered by an eight-pole low-pass Bessel filter (model 900, Frequency Devices, Haverhill, MA) at a frequency of 10 kHz and sampled at 50 kHz. The rise time of the filter $T_r = 339/f_c$, where f_c is the corner frequency of the low-pass Bessel filter.[27,28] For an f_c value of 500 Hz, we obtain a T_r of ∼680 μs. This value would give us a dead time T_d of $0.54T_r$ (=365 μs). Employing single-channel analysis of the missed events,[29−31] we estimated that the missed current blockades were not more than 8% of the total number of events in each recorded trace.

Temperature Controller for Single-Channel Electrical Recordings with Planar Lipid Bilayers. The temperature control experiments were conducted using a Dagan HCC-100A controller (Dagan Corp., Minneapolis, MN), which was adapted to planar bilayer recordings.[32,33] The temperature was simultaneously monitored in the aluminum stage holding the bilayer chamber as well as in the bilayer chamber with thermocouple probes.

Molecular Graphics. The OccK1 protein model was generated with Chimera[34] using Protein Data Bank entry 2qtk.[24]

RESULTS

Exploring the Optimal Experimental Conditions for Temperature-Dependent, Single-Channel Analysis. Single-channel examination of the temperature dependence of the current fluctuations among the three open substates required a careful consideration of the experimental conditions.[35,36] We decided to employ an ionic aqueous phase containing 2 M KCl for amplifying the signal-to-ratio noise, such as in the previous work with temperature-responsive, loop-containing α-hemolysin protein nanopores.[32] Importantly, the number of open substates remains preserved by altering the salt concentration of the aqueous phase from 1 to 4 M KCl.[18] In addition, there is no substantial change in the kinetic rate constants when the salt concentration was varied from 1 to 2 M KCl.

A second issue is the choice of the buffer. Most buffers are unstable under different temperature regimes, meaning that there are substantial changes in pH accompanying changes in temperature. To cancel all the temperature-dependent factors that affect pH, we used a buffer with a low temperature coefficient.[37,38] One excellent candidate, already tested in prior temperature-dependent single-channel experiments, is potassium phosphate.[32,33,39] However, one possibility is that the presence of the potassium phosphate buffer alters the single-channel electrical signature of the OccK1 protein channel. To test this hypothesis, we pursued titration experiments with potassium phosphate buffer. Using various potassium phosphate concentrations, in the range of 2−20 mM, we were not able to detect statistically significant changes in the dwell time of all open substates, O_1−O_3 (Supporting Information, Figure

dx.doi.org/10.1021/bi300332z | *Biochemistry* 2012, 51, 5348−5358

S1), indicating no effect of the buffer on the single-channel kinetics.

All our temperature-dependent single-channel electrical recordings were performed at pH 7.4. However, how is the single-channel electrical signature impacted by pH? The potassium phosphate buffer operates well in the pH range of 6−8.[37,40] Therefore, we executed single-channel electrical recordings with OccK1 at pH 6 and 8. Interestingly, we found no statistically significant alterations of the dwell times of open substates O_1−O_3. Representative single-channel electrical recordings are shown in Figure 2. In 1 M KCl and 10 mM potassium phosphate (pH 6), the fitted dwell times of the O_1−O_3 open substates were 1.8 ± 0.3, 7.6 ± 0.1, and 3.9 ± 0.2 ms, respectively. Under similar experimental conditions, the values of these dwell times, determined at pH 8, were 2.1 ± 0.2, 6.9 ± 0.2, and 3.6 ± 0.2 ms, respectively. These results indicate a lack of chargeable groups within the channel lumen under inspected experimental circumstances (pH 6−8). We examined the high-resolution X-ray crystal structure of the OccK1 protein and found that indeed histidine residues (pK_a = 6) are located outside the channel lumen.[23]

Changing pH to either a more alkaline or a more acidic value requires a replacement of the potassium phosphate buffer. Therefore, we performed single-channel electrical recordings at pH 3 in 10 mM potassium acetate and at pH 9.0 in 10 mM Tris-HCl. The data were collected with an aqueous phase containing 1 M KCl. Typical single-channel traces are illustrated in Figure 3. In both cases, we determined a large number of nonresolvable single-channel current blockade events. Moreover, we found that the open substate current levels were not well-defined at acidic pH. Therefore, a neutral pH obtained with a potassium phosphate buffer is a robust choice for temperature-dependent single-channel recordings.

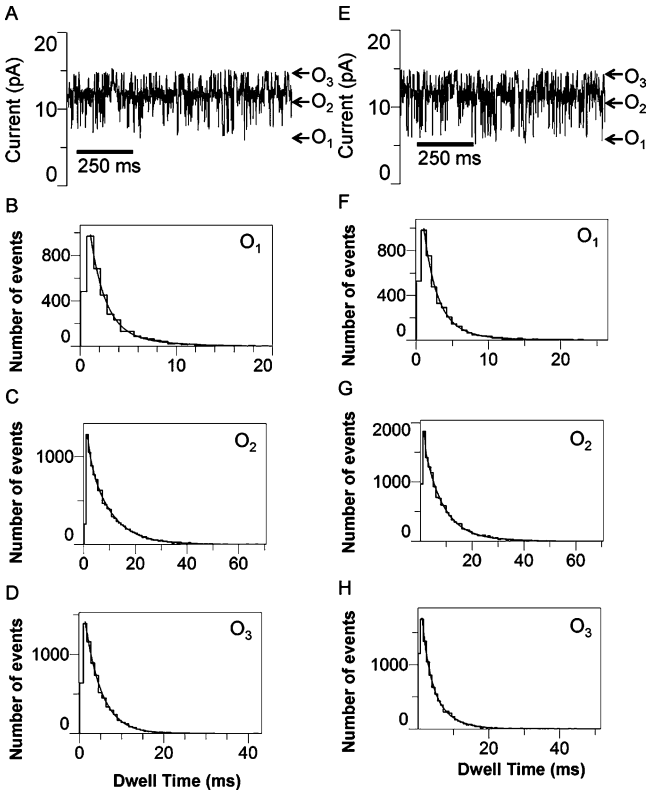

Figure 2. Representative single-channel electrical recordings acquired with the OccK1 protein at different pH values. (A) Typical single-channel electrical trace recorded at pH 6.0. (B) Dwell-time histogram of the O_1 events from panel A. (C) Dwell-time histogram of the O_2 events from panel A. (D) Dwell-time histogram of the O_3 events from panel A. (E) Typical single-channel electrical trace recorded at pH 8.0. (F) Dwell-time histogram of the O_1 events from panel E. (G) Dwell-time histogram of the O_2 events from panel E. (H) Dwell-time histogram of the O_3 events from panel E. The fits were based upon log likelihood ratio (LLR) tests with a given confidence level of 0.95.[46,69] The results of the fits were as follows: (B) τ_{O_1} = 1.8 ± 0.3 ms, (C) τ_{O_2} = 7.6 ± 0.1 ms, (D) τ_{O_3} = 3.9 ± 0.2 ms, (F) τ_{O_1} = 2.1 ± 0.2 ms, (G) τ_{O_2} = 6.9 ± 0.2 ms, and (H) τ_{O_3} = 3.6 ± 0.2 ms. For the sake of clarity, the single-channel electrical traces were low-pass Bessel filtered at 500 Hz. The buffer solution contained 1 M KCl and 10 mM potassium phosphate at room temperature. The applied transmembrane potential was 40 mV.

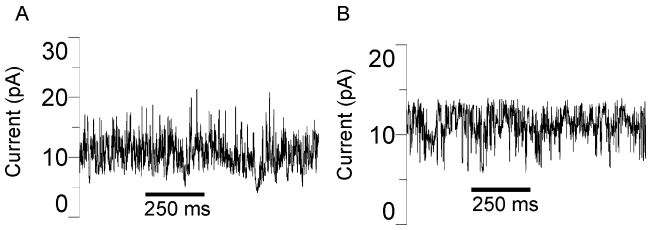

Figure 3. Typical single-channel electrical recordings with the OccK1 protein channel at acidic and alkaline pH values. (A) Representative trace acquired at pH 3.0 in 10 mM potassium acetate buffer. (B) Representative trace recorded at pH 9.0 in 10 mM Tris-HCl buffer. The aqueous phase contained 1 M KCl. The applied transmembrane potential was 40 mV. For the sake of clarity, the single-channel electrical traces were low-pass Bessel filtered at 500 Hz.

Temperature Dependence of the Single-Channel Electrical Recordings with the OccK1 Protein. The OccK1 protein was expressed and purified by standard protein chemistry techniques (Supporting Information, Figure S2). We examined OccK1 in a temperature regime below room temperature, between 4 and 20 °C. This strategy allowed a detailed single-channel analysis of all current fluctuations observed in a previous work performed at room temperature.[18] This experimental design was motivated by the fact that the kinetic rate constants were expected to substantially increase at elevated temperatures, reaching values beyond the resolution of our instrument. In Figure 4A, we show a typical single-channel electrical trace recorded with wild-type OccK1 (WT-OccK1) at 20 °C and at an applied transmembrane potential of 40 mV. Clearly, this trace displays three major open substates (O_1−O_3) that were further explored using standard dwell-time histograms (Figure 4B−D). A similar number of substates were found at an applied transmembrane potential of −40 mV (Supporting Information, Figure S3), permitting direct meaningful comparisons among data recorded at both negative and positive voltage biases.

These three current substate levels were determined using both fitted current amplitude histograms (Supporting Information, Figure S4) and all-points current amplitude histograms (Supporting Information, Figure S5). The number of open substates was also conserved at 4 °C (Figure 4E−G). No O_1 to O_3 or O_3 to O_1 transition was observed in this work, indicating a linear kinetic scheme with three distinguishable open substates ($O_1 \leftrightarrow O_2 \leftrightarrow O_3$), and with the most probable

dx.doi.org/10.1021/bi300332z | Biochemistry 2012, 51, 5348−5358

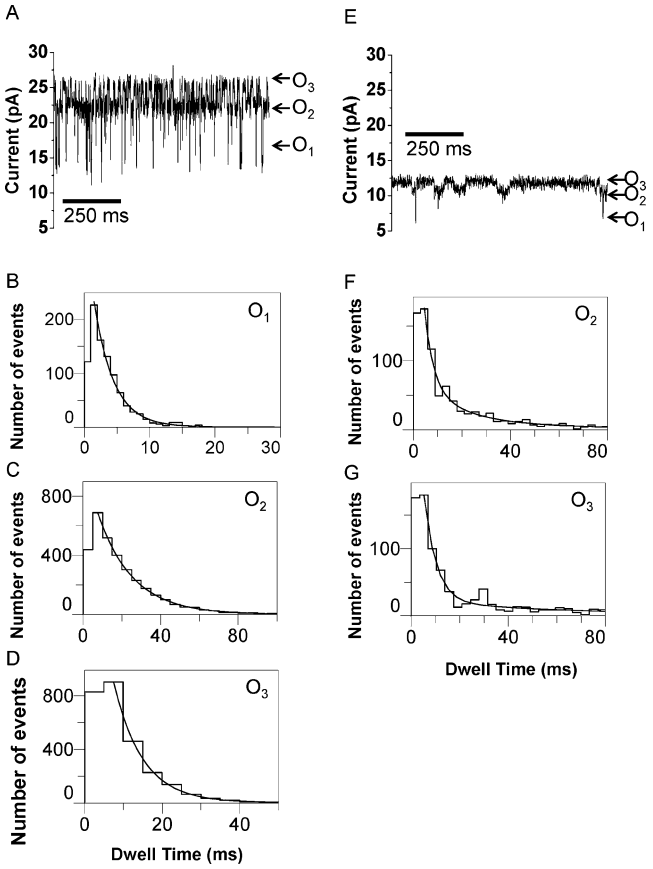

Figure 4. Representative single-channel electrical recordings acquired with the WT-OccK1 protein at different temperatures. (A) Typical single-channel electrical trace recorded at 20 °C. (B) Dwell-time histogram of the O_1 events from panel A. (C) Dwell-time histogram of the O_2 events from panel A. (D) Dwell-time histogram of the O_3 events from panel A. (E) Typical single-channel electrical trace recorded at 4 °C. (F) Dwell-time histogram of the O_2 events from panel E. (G) Dwell-time histogram of the O_3 events from panel E. The fits were based upon a log likelihood ratio (LLR) test with a given confidence level of 0.95. The results of the fits were as follows: (B) τ_{O_1} = 6.3 ± 1.1 ms, (C) τ_{O_2} = 17.5 ± 0.1 ms, (D) τ_{O_3} = 7.4 ± 0.1 ms, (F) τ_{O_2} = 28.3 ± 6.1 ms, and (G) τ_{O_3} = 32.17 ± 8.4 ms. At 4 °C, the number of O_1 events was not satisfactory for the construction of a standard dwell-time histogram, so a different protocol for the single-channel analysis of individual O_1 events was employed. The single-channel electrical traces were low-pass Bessel filtered at 500 Hz. The transmembrane potential was 40 mV. The buffer solution consisted of 2 M KCl and 10 mM potassium phosphate (pH 7.4).

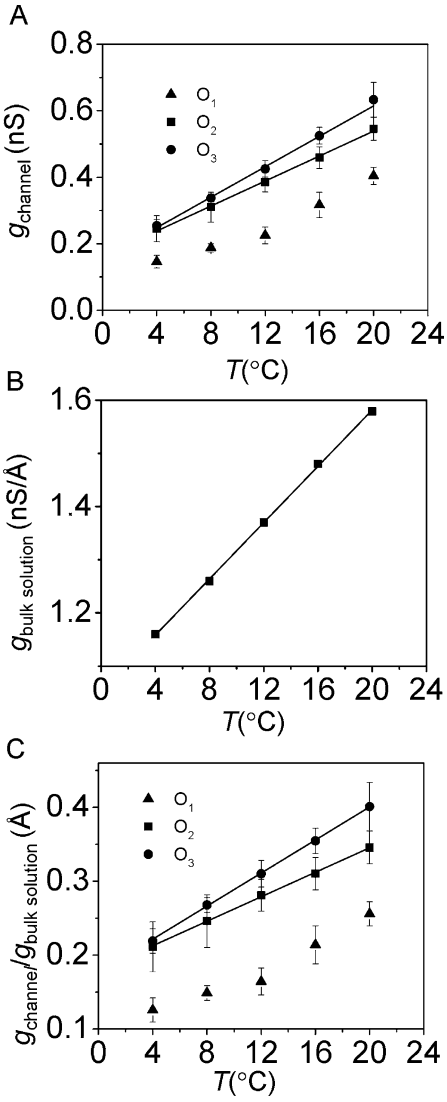

Figure 5. Temperature dependence of the single-channel conductance of the OccK1 protein channel. (A) Single-channel conductance of the three open substates of the OccK1 protein channel. (B) Conductivity of a 2 M KCl solution as a function of temperature, in 10 mM potassium phosphate (pH 7.4). (C) Single-channel conductance of the three open substates of the OccK1 protein channel normalized to the conductivity of the bulk aqueous phase from panel B. The applied transmembrane potential was 40 mV.

O_2 open substate at 20 °C, from which reversible transitions to the flanked open substate O_1 and O_3 levels occurred.

Temperature Dependence of the Unitary Conductance of the OccK1 Protein Channel. We pursued the effect of temperature on the unitary conductance associated with each open substate recorded in single-channel traces with the OccK1 protein channel. These data sets are illustrated in Figure 5. While the unitary conductance of the O_2 and O_3 open substates underwent a linear increase with an increase in temperature, with slopes of ~0.018 and ~0.022 nS/°C, respectively, the conductance value corresponding to the low-conductance O_1 open substate displayed a rectified enhancement (Figure 5A). We normalized the unitary conductance [$g_{channel}$ (Figure 5A)] to the conductivity of the bulk aqueous phase [$g_{bulk\ solution}$ (Figure 5B)]. Again, the normalized conductance values of the O_2 and O_3 open substates followed a linear increase with temperature, whereas the normalized conductance value corresponding to the low-conductance O_1 open substate increased steeply at elevated temperatures (Figure 5C). Therefore, for the three open substates, the slope of the unitary conductance with an increasing temperature is greater than the slope of the conductivity of the bulk aqueous phase.

Determination of the Kinetic Rate Constants. These kinetic rate constants were calculated using the event frequencies (f) and the average dwell times (τ) of the flanked O_1 and O_3 substates.[18] Using standard chemical kinetics formalisms for single-molecule fluctuations of the OccK1 protein channel,[41] we formulated the following system of partial differential equations:[42−44]

dx.doi.org/10.1021/bi300332z | Biochemistry 2012, 51, 5348−5358

$$\frac{dP_{O_1}}{dt} = -k_{O_1\to O_2}P_{O_1} + k_{O_2\to O_1}P_{O_2}$$
$$\frac{dP_{O_2}}{dt} = +k_{O_1\to O_2}P_{O_1} - k_{O_2\to O_1}P_{O_2} + k_{O_3\to O_2}P_{O_3} - k_{O_2\to O_3}P_{O_2}$$
$$\frac{dP_{O_3}}{dt} = -k_{O_3\to O_2}P_{O_3} + k_{O_2\to O_3}P_{O_2} \quad (1)$$

where P_{O_1}, P_{O_2}, and P_{O_3} are the probabilities to occupy the O_1−O_3 open substates, respectively. These probabilities are given by the following expressions:[42−44]

$$P_{O_1} = \frac{T_{O_1}}{T} = \frac{N_{O_1}\tau_{O_1}}{T} = f_{O_1}\tau_{O_1}$$
$$P_{O_2} = \frac{T_{O_2}}{T} = \frac{N_{O_2}\tau_{O_2}}{T} = (f_{O_1} + f_{O_3})\tau_{O_2}$$
$$P_{O_3} = \frac{T_{O_3}}{T} = \frac{N_{O_3}\tau_{O_3}}{T} = f_{O_3}\tau_{O_3} \quad (2)$$

where T_{O_1}, T_{O_2}, and T_{O_3} are the total times occupied by the O_1−O_3 open substates, respectively. N_{O_1}, N_{O_2}, and N_{O_3} are the total numbers of recorded events that correspond to the O_1−O_3 substates, respectively. T indicates the total recording time. f and τ denote the event frequency and the average dwell time for an open substate, respectively. Equations 2 indicate two components for the O_2 open substate, corresponding to the transitions toward the O_1 and O_3 open substates. The well made by the O_2 open substate is flanked by two barriers for reaching the O_1 and O_3 open substates.

The rates for reaching the O_1 and O_3 open substates are just the corresponding event frequencies, which are normalized to the P_{O_2} probability:

$$k_{O_2\to O_1} = \frac{f_{O_1}}{P_{O_2}} = \frac{f_{O_1}}{1 - f_{O_1}\tau_{O_1} - f_{O_3}\tau_{O_3}}$$
$$k_{O_2\to O_3} = \frac{f_{O_3}}{P_{O_2}} = \frac{f_{O_3}}{1 - f_{O_1}\tau_{O_1} - f_{O_3}\tau_{O_3}} \quad (3)$$

At equilibrium, the partial derivatives of eqs 1 are zero, because the event probabilities are constant. Therefore

$$k_{O_1\to O_2} = \frac{1}{\tau_{O_1}}$$
$$k_{O_3\to O_2} = \frac{1}{\tau_{O_3}} \quad (4)$$

Equations 3 and 4 indicate that the four kinetic rate constants, which describe the kinetic scheme with three open substates, can be calculated using the event frequencies and the average dwell times of the flanked O_1 and O_3 open substates. Moreover, equations 3 and 4 confirm the general rule that the average dwell time of a certain open substate is given by the reciprocal of the sum of the kinetic rate constants for the transitions occurring away from that respective open substate:[33,41,45,46]

$$\frac{1}{\tau_{O_2}} = k_{O_2\to O_1} + k_{O_2\to O_3} \quad (5)$$

The temperature dependence of the kinetic rate constants underwent a linear dependence in a semilog Arrhenius representation (Figure 6A; Supporting Information, Figure S6). As expected, $k_{O_2\to O_1}$, $k_{O_2\to O_3}$, and $k_{O_3\to O_2}$ increased with an increase in temperature. Surprisingly, $k_{O_1\to O_2}$ decreased at elevated temperatures.

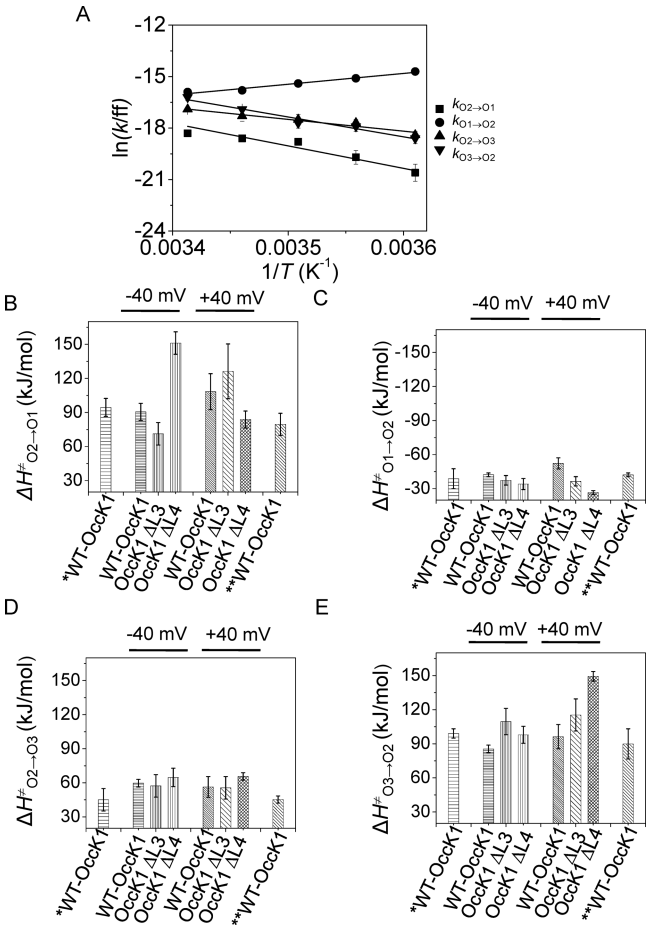

Figure 6. Determination of thermodynamic parameters using semilog Eyring plots. (A) Dependence of the four kinetic rate constants of the WT-OccK1 protein vs the reciprocal of the absolute temperature at an applied transmembrane potential of 40 mV. All experimental conditions were similar to those shown in Figure 5. Panels B−E show activation free enthalpies of all single-channel current transitions. In panels B−E, vertical bars marked by *WT-OccK1 and **WT-OccK1 indicate the activation free enthalpies inferred from single-channel data acquired at applied transmembrane potentials of −60 and 60 mV, respectively.

Rational Design of the Loop-Deletion OccK1 Proteins.

We asked whether deletions of major extracellular loops L3, L4, and L7 impacts the temperature-dependent kinetics and energetics of the current fluctuations (Supporting Information, Table S2 and Figures S6−S9). We made loop-deletion OccK1 proteins based upon inspection of the high-resolution structure of WT-OccK1.[22] These mutants were designed with the first requirement that the residues immediately before and after the deletion be close enough in space that they could be replaced by a single glycine residue without introducing significant

dx.doi.org/10.1021/bi300332z | Biochemistry 2012, 51, 5348−5358

Table 1. Equilibrium Free Energies, Enthalpies, and Entropies of WT-OccK1, OccK1 ΔL3, and OccK1 ΔL4

voltage (mV)	protein	$\Delta H^\circ_{O_1\rightarrow O_2}$ (kJ/mol)	$\Delta S^\circ_{O_1\rightarrow O_2}$ (J mol^{-1} K^{-1})	$\Delta G^\circ_{O_1\rightarrow O_2}{}^a$ (kJ/mol)	$\Delta G^\circ_{O_1\rightarrow O_2}{}^b$ (kJ/mol)	$\Delta H^\circ_{O_3\rightarrow O_2}$ (kJ/mol)	$\Delta S^\circ_{O_3\rightarrow O_2}$ (J mol^{-1} K^{-1})	$\Delta G^\circ_{O_3\rightarrow O_2}{}^a$ (kJ/mol)	$\Delta G^\circ_{O_3\rightarrow O_2}{}^b$ (kJ/mol)
40	WT-OccK1	−161 ± 21	−533 ± 167	−15.1 ± 2.3	−1.8 ± 0.2	40 ± 2	139 ± 5	2.1 ± 0.2	−1.4 ± 0.1
40	OccK1 ΔL3	−163 ± 28	−541 ± 99	−14.9 ± 1.3	−1.5 ± 0.6	60 ± 4	215 ± 12	1.1 ± 0.8	−4.2 ± 0.6
40	OccK1 ΔL4	−110 ± 9	−357 ± 32	−12.9 ± 0.6	−4.0 ± 0.1	52 ± 3	179 ± 8	1.6 ± 0.7	−2.7 ± 0.5
−40	WT-OccK1	−133 ± 9	−431 ± 32	−15.2 ± 0.5	−4.4 ± 0.3	25 ± 1	91 ± 12	1.7 ± 0.2	−1.5 ± 0.7
−40	OccK1 ΔL3	−109 ± 14	−365 ± 14	−13.4 ± 2.5	−3.2 ± 0.4	52 ± 2	184 ± 5	2.0 ± 0.3	−2.6 ± 0.1
−40	OccK1 ΔL4	−185 ± 15	−613 ± 54	−18.0 ± 0.1	−2.6 ± 0.3	33 ± 1	116 ± 5	1.5 ± 0.7	−1.4 ± 0.8

[a]Data were calculated at 0 °C. [b]Data were calculated at 25 °C.

conformational perturbations of the altered loop. Single-channel data with a loop deletion in L7 (OccK1 ΔL7, S281−G287), which lacks an intramolecular R284−D116 salt bridge between loops L7 and L3, showed a noisy electrical signature, which was the reason not to pursue further temperature-dependent single-channel electrical recordings with this mutant.[24] However, this mutant showed a most probable conductance greater than the unitary conductance of WT-OccK1, confirming that loop L7 is indeed exposed to the channel lumen. We also constructed deletion mutant OccK1 ΔL3 (D124−P129), which, in the high-resolution crystal structure,[22] lacks an intramolecular D124−R16 salt bridge between loop L3 and the pore wall (Supporting Information, Table S2 and Figures S7 and S8). In addition, we examined the OccK1 ΔL4 deletion mutant (L166−K175), which does not contain any salt bridge. A second criterion for the selection of deletion-loop OccK1 mutants was that the single-channel conductance and the number of the open substates be similar to those of the WT-OccK1 protein, so a meaningful temperature-dependent comparison of kinetic and thermodynamic parameters among them was possible. While the OccK1 ΔL7 protein did not fulfill the second criterion, OccK1 ΔL3 and OccK1 ΔL4 exhibited a closely similar unitary conductance and a number of open substates identical to that of WT-OccK1 (Supporting Information, Figure S9). It is worth mentioning that these loop-deletion OccK1 mutants lack several hydrogen bonds as well as van der Waals interactions with other loops (L2, L3, L6, and L7) and the β-barrel pore wall (Supporting Information, Table S2).

Enthalpic and Minimal Entropic Contributions to the Gating Transitions of the OccK1 Proteins. Using linear semilog Eyring plots of the kinetic rate constants versus the reciprocal of the absolute temperature, we determined the enthalpic ($\Delta H^\ddagger$) and entropic ($\Delta S^\ddagger$) contributions to the activation free energies ($\Delta G^\ddagger$):[39,47−49]

$$\ln k = \ln \mathrm{ff} + \frac{\Delta S^\ddagger}{R} - \frac{\Delta H^\ddagger}{R} \times \frac{1}{T} \qquad (6)$$

where ff = $k_B T/h$ (6×10^{12} s^{-1}) is the Eyring frequency factor for the gas phase. k_B, T, and h are Boltzmann's constant, the absolute temperature, and Planck's constant, respectively. The ff parameter is much smaller for conformational transitions of proteins in the aqueous phase.[50] Eyring transition state theory (TST) was first used for elementary chemical reactions in the gas phase. In this work, we did not use or assume a frequency factor for quantitative determinations of the activation free enthalpies as well as equilibrium free energies, enthalpies, and entropies (see below). However, we employed TST formalism for the phenomenological exponential dependence of the kinetic rate constants on the activation free energies, which is routinely used in single-channel electrical data analysis.[39,42,50−55] It is also true that the extension of TST to the condensed phase by Hänggi involved complicated expressions of the frequency factor.[56] This result makes TST impractical for accurate quantitative determinations of the entropic contribution to the activation free energy in single-channel kinetics and protein folding.[53]

Determinations of $\Delta H^\ddagger$ were made directly using the slope $-\Delta H^\ddagger/R$ of the semilog k plots (Figure 6A; Supporting Information, Table S3). They were based on the assumption that the thermodynamic parameters $\Delta H^\ddagger$ and $\Delta S^\ddagger$ are not temperature-dependent in the temperature range examined in this work.[57] The uncertainty of ff produces inaccuracy in calculating the exact values of $\Delta G^\ddagger$ and $\Delta S^\ddagger$. However, knowing that ff < 6×10^{12} s^{-1} for protein transitions in the aqueous phase, we can obtain an estimate of the maximal value of the activation free energy [$\Delta G^\ddagger_{max} = RT \times \ln(\mathrm{ff}/k)$] and the lower limit of the activation entropy [$\Delta S^\ddagger_{min} = (\Delta H^\ddagger - \Delta G^\ddagger_{max})/T$] (Supporting Information, Table S4).[54]

Figure 6 illustrates the effect of the loop deletion on the transition enthalpy as well as the impact of the sign of the 40 mV voltage. The large-amplitude $O_2 \rightarrow O_1$ current transitions showed a favorable enthalpic contribution (Figure 6B; Supporting Information, Table S3), which was compensated by unfavorable entropic contributions. For WT-OccK1, at 40 mV and 20 °C, the minimal entropic contribution and the maximal activation free energy were −42 ± 6 kJ/mol ($-T\Delta S^\ddagger_{O_2\rightarrow O_1\text{-min}}$) and 66 ± 10 kJ/mol ($\Delta G^\ddagger_{O_2\rightarrow O_1\text{-max}}$), respectively (Supporting Information, Table S4). In contrast to the $O_2 \rightarrow O_1$ transition, the large-amplitude $O_1 \rightarrow O_2$ current fluctuations were characterized by a negative activation enthalpy (Figure 6C). This large-amplitude, $O_1 \rightarrow O_2$ current transition showed a substantially favorable entropic contribution, with a $-T\Delta S^\ddagger_{O_1\rightarrow O_2\text{-min}}$ value of 119 ± 15 kJ/mol, giving a maximal free energy of activation ($\Delta G^\ddagger_{O_1\rightarrow O_2\text{-max}}$) of 60 ± 10 kJ/mol at 40 mV and 20 °C. At a voltage of 40 mV, a distinctive feature of the small-amplitude $O_2 \rightarrow O_3$ current transition is that its $\Delta H^\ddagger$ was not impacted by either the sign of the voltage or the deletions operating in loop L3 or L4 (Figure 6D). However, the $\Delta H^\ddagger$ for the $O_2 \rightarrow O_3$ transition of the OccK1 protein channel was decreased at applied transmembrane potentials of 60 and −60 mV, revealing the complexity of the

dx.doi.org/10.1021/bi300332z | Biochemistry 2012, 51, 5348−5358

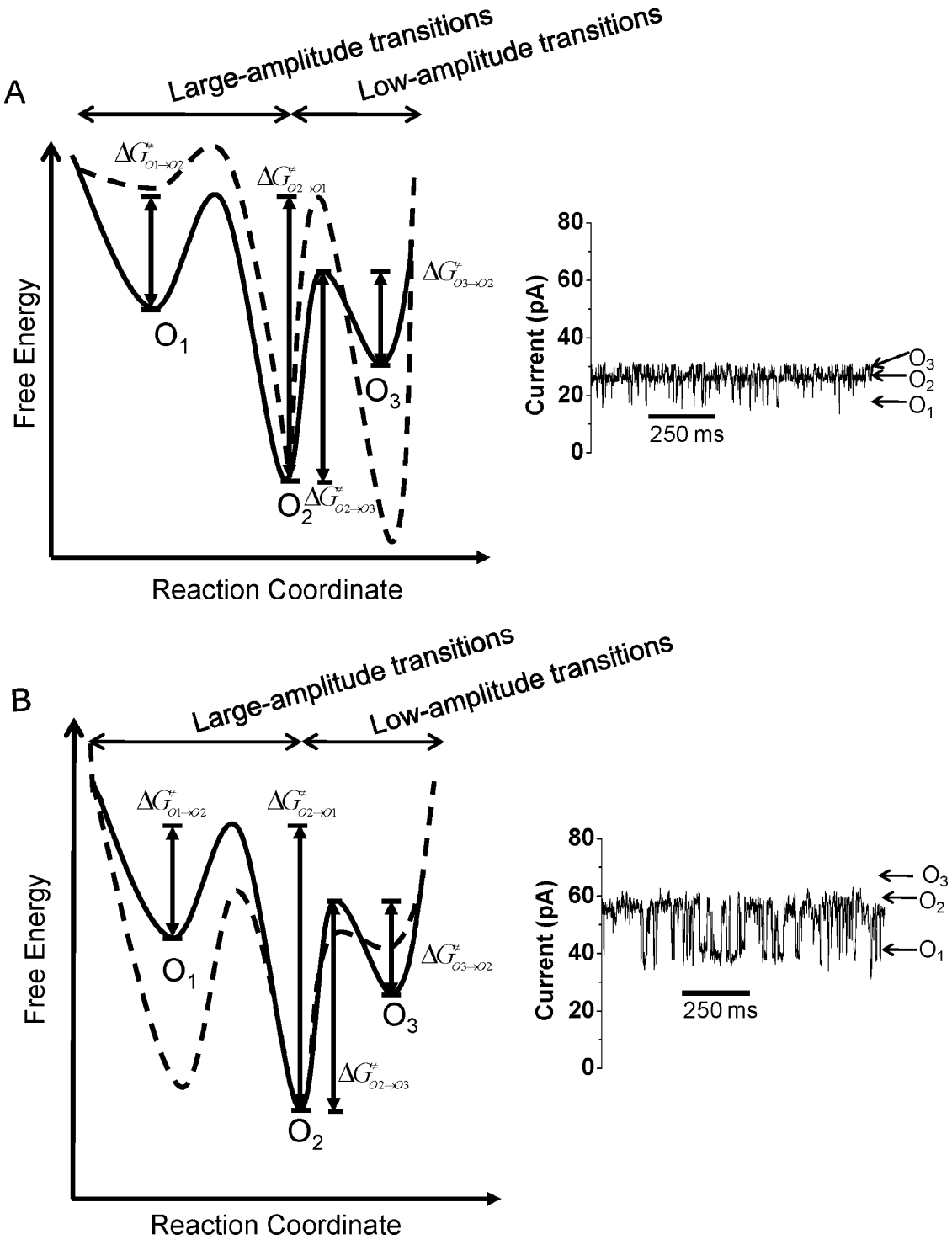

Figure 7. Alterations in the free energy landscape of the WT-OccK1 protein due to modifications of temperature. (A) The solid line is the free energy landscape at 20 °C, whereas the dashed line is the free energy landscape at 4 °C. (B) The solid line is the free energy landscape at 20 °C, whereas the dashed line corresponds to the free energy landscape at 50 °C. The single-channel electrical traces on the right-hand side show a comparison between the electrical signatures acquired at 20 (A) and 50 °C (B). In panel B, the O_3 events, if present, were much shorter than the time resolution of the experiment, so they were not detectable. The other experimental conditions were the same as in Figure 5. The reaction coordinate is the position of the fluctuating part of the OccK1 protein with respect to the trans opening.

voltage dependence of this transition. The small-amplitude $O_3 \rightarrow O_2$ current transition exhibited a fairly large enthalpic contribution, in the range of 86−149 kJ/mol (Figure 6E), and was affected by deletions in loops L3 and L4. For example, at 40 mV, the absolute magnitude of $\Delta H^{\ddagger}_{O_3 \rightarrow O_2}$ increased in the following order: WT-OccK1 < OccK1 ΔL3 < OccK1 ΔL4 (Figure 6C; Supporting Information, Table S3).

Energetics of the Current Fluctuations. The equilibrium free energies ($\Delta G°$), enthalpies ($\Delta H°$), and entropies ($\Delta S°$) from open substate O_1 or O_3 to open substate O_2 were calculated using the fits of the ratio between corresponding

dx.doi.org/10.1021/bi300332z | *Biochemistry* 2012, 51, 5348−5358

kinetic rate constants, which is similar to a van't Hoff equation:[58,59]

$$\ln\left(\frac{k_{O_1\rightarrow O_2}}{k_{O_2\rightarrow O_1}}\right) = \left(-\frac{\Delta H^{\circ}_{O_1\rightarrow O_2}}{R}\right)\frac{1}{T} + \frac{\Delta S^{\circ}_{O_1\rightarrow O_2}}{R}$$

$$\ln\left(\frac{k_{O_3\rightarrow O_2}}{k_{O_2\rightarrow O_3}}\right) = \left(-\frac{\Delta H^{\circ}_{O_3\rightarrow O_2}}{R}\right)\frac{1}{T} + \frac{\Delta S^{\circ}_{O_3\rightarrow O_2}}{R} \quad (7)$$

The large-amplitude current transitions of the WT-OccK1 protein were characterized by a highly favorable enthalpic contribution [−161 ± 21 kJ/mol (Table 1)]. This value is on the order of ≥8 hydrogen bonds (ΔH_{HB} ∼ 8−20 kJ/mol), indicating that the channel transition is accompanied by large conformational alterations of the extracellular loops blocking the channel lumen. This highly favorable enthalpic component was balanced by a large entropic penalty (−533 ± 167 J mol^{-1} K^{-1}), giving a small equilibrium free energy at 25 °C [−1.8 ± 0.2 kJ/mol (Table 1)]. OccK1 ΔL3 featured closely similar thermodynamic parameters at 40 mV. In contrast, these findings for the $O_1 \leftrightarrow O_2$ transitions were reversed at −40 mV; namely, the $\Delta H^{\circ}_{O_1\rightarrow O_2}$ of OccK1 ΔL4 was greater than the values corresponding to WT-OccK1 and OccK1 ΔL3. The energetic barrier between the O_2 and O_3 open substates of the WT-OccK1 protein showed a favorable entropic component $\Delta S^{\circ}_{O_3\rightarrow O_2}$ of 139 ± 5 J mol^{-1} K^{-1} at a transmembrane potential of 40 mV. This favorable entropic contribution was compensated by an unfavorable enthalpic contribution $\Delta H^{\circ}_{O_3\rightarrow O_2}$ of 40 ± 2 kJ/mol, producing a small equilibrium free energy at 25 °C [$\Delta G^{\circ}_{O_3\rightarrow O_2}$ = −1.4 ± 0.1 kJ/mol (Table 1)]. OccK1 ΔL3 and OccK1 ΔL4 exhibited increased unfavorable enthalpic contributions of 60 ± 4 and 52 ± 3 kJ/mol but more favorable and compensating entropic components of 215 ± 12 and 179 ± 8 J mol^{-1} K^{-1}, respectively. Similarly, at −40 mV, as compared to WT-OccK1, OccK1 ΔL3 and OccK1 ΔL4 showed greater favorable entropic contributions of 184 ± 5 and 116 ± 5 J mol^{-1} K^{-1}, respectively, which were compensated by unfavorable enthalpic contributions of 52 ± 2 and 33 ± 1 kJ/mol, respectively (Table 1).

DISCUSSION

Because we were not able to detect direct $O_1 \rightarrow O_3$ and $O_3 \rightarrow O_1$ transitions, we judge that the large-amplitude current fluctuations and small-amplitude current fluctuations were made by distinct parts of the WT-OccK1 protein within the channel lumen. This characteristic of the WT-OccK1 protein is advantageous, because the temperature-dependent, single-channel analysis can be easily pursued for individual transitions that are independent of each other. Interestingly, we determined that the temperature dependence of the single-channel conductance of the OccK1 protein is different from that of the effective conductance given by the bulk aqueous phase. For example, increasing the temperature produced an amplification of the ratio between the single-channel conductance and the bulk conductivity. Remarkably, similar results were obtained in prior temperature-dependent, single-channel studies with the outer membrane proteins C (OmpC) and F (OmpF) of *E. coli*.[60,61] Chimerel and co-workers argued that two possible mechanisms are responsible for this observed phenomenon: the dynamics of the surface charges and the lifetime of the ion pairs within the channel lumen.[60] For example, the confined nature of the channel lumen catalyzes the formation of more ion pairs inside the channel lumen than outside it. Elevating the temperature drastically decreases the lifetime of the ion pairs, which favors an increase in the single-channel conductance that is steeper than that expected from the bulk aqueous phase.

The most probable open substate at 20 °C was O_2, from which the system departed to either the O_1 open substate crossing an enthalpic barrier or the O_3 open substate crossing an entropic barrier. The former fluctuation is a large-amplitude current transition that is characterized by a large activation enthalpy ($\Delta H^{\ddagger}_{O_2\rightarrow O_1}$ = 108 ± 16 kJ/mol), whereas the latter fluctuation is a small-amplitude current transition featuring a smaller activation enthalpy ($\Delta H^{\ddagger}_{O_2\rightarrow O_3}$ = 56 ± 9 kJ/mol). The free energy landscape model corresponding to a temperature of 4 °C is illustrated in Figure 7A (left panel, dashed line). In this case, the most probable open substate is no longer O_2, so there is a switch in the gating profile of the WT-OccK1 protein between the O_2 and O_3 open substates. The gradual shift of the O_3 open substate at more negative free energies at lower temperatures was accompanied by a progressive drift of the O_1 substate at less negative free energies. Therefore, the O_1 and O_3 open substates displayed reversal behavior with respect to the changes in temperature in the chamber.

On the basis of the single-channel data acquired at low temperatures, we predicted that at elevated temperatures all activation free energies, except $\Delta G^{\ddagger}_{O_1\rightarrow O_2}$, will decrease with an increase in temperature (Figure 7B, left panel, dashed line). Indeed, the event frequency and duration of the O_1 current blockades increased at 50 °C (Figure 7B, right panel). Moreover, we were not able to detect the small-amplitude $O_2 \leftrightarrow O_3$ current fluctuations, again confirming that these events occurred with a duration much faster than that of the time resolution of our instrument. It is also conceivable that most of these transitions will be missed at elevated temperatures, because of their low current amplitude. The lack of the small-amplitude current transitions corroborates the model prediction for substantially decreased activation free energy $\Delta G^{\ddagger}_{O_3\rightarrow O_2}$ (Figure 7B, left panel, dashed line).

Another interesting aspect of these results is the counter-intuitive negative value of $\Delta H^{\ddagger}_{O_1\rightarrow O_2}$, which resulted from an increase in the microscopic $k_{O_1\rightarrow O_2}$ transition rate constant at lower temperatures. We judge that this finding is counter-intuitive, because it used to be thought that the rates of chemical reactions become faster with an increase in temperature. What is the reason for this anomaly? The $O_1 \rightarrow O_2$ gating transition is accompanied by a strongly negative $\Delta S^{\ddagger}_{O_1\rightarrow O_2}$ ($\Delta S^{\ddagger}_{O_1\rightarrow O_2\text{-min}}$ = −405 ± 52 J mol^{-1} K^{-1}). This drastic decrease in the activation entropy might be produced by a local formation of intramolecular interactions during the conformational alterations accompanying the transition process. Here, we report for the first time that the gating fluctuations of a β-barrel protein channel undergo a negative activation enthalpy. It was long believed that negative activation energies of reactions are governed by barrierless transitions, in which the reactive molecule is captured in a potential well. In our system, we show the presence of a barrier between O_1 and O_2, $\Delta G^{\ddagger}_{O_1\rightarrow O_2}$, whose energetic value decreases at lower temperatures. Oliveberg and colleagues explained that large-scale conforma-

dx.doi.org/10.1021/bi300332z | *Biochemistry* 2012, 51, 5348−5358

tional transitions of proteins represent highly dimensional reactions between many residues and solvent molecules, which under some experimental circumstances may feature negative activation enthalpies.[57] Recently, other groups determined negative activation enthalpies accompanying the kinetics of protein folding.[62,63] Noronha and colleagues, using a combination of rapid-mixing temperature jump and laser temperature jump with fluorescence detection, determined that the activation enthalpy of folding required for a 76-residue ubiquitin-based polypeptide is approximately −45 kJ/mol.[63]

Detailed comparison analysis of the four current transitions observed with WT-OccK1, OccK1 ΔL3, and OccK1 ΔL3 revealed statistically significant distinctions in the transition enthalpies as well as equilibrium free energies, enthalpies, and entropies of these proteins. One immediate question is why these single-channel current fluctuations display large activation enthalpies. A transmembrane protein channel, such as many other proteins, exhibits remarkable temperature dependence. In fact, any protein is a great temperature sensor. The Q_{10} temperature coefficient of the OccK1 protein channel, which is defined as the kinetic rate constant measured at temperature T + 10 divided by the kinetic rate constant measured at temperature T (k_{T+10}/k_T), covered a range between 2 and 6 for all inspected transitions. The current gating of a protein channel has typical Q_{10} values in the range of 2−4.[53,64−66] If Q_{10} is 4, this value corresponds to an activation enthalpy of $\sim 43 k_B T$. Then, how is it possible to have thermally induced current fluctuations characterized by an enormous activation enthalpy, which is much greater than $k_B T$? The probability of such a transition would be very small, so the transition would be barely detectable. However, it happens that such thermally induced current transitions feature compensatory entropic contributions to the activation free energy. Large enthalpic modifications ($\Delta H^{\ddagger}$) to the transition energies are accompanied by large, compensating entropic alterations ($-T\Delta S^{\ddagger}$), which result in smaller $\Delta G^{\ddagger}$ values. Enthalpy−entropy compensation is a general property in many chemical reactions, protein folding, and all processes dominated by weak interactions.[67] The OccK1 protein channel comprises large extracellular loops L3, L4, and L7 folded back into the channel lumen (Supporting Information, Table S1). These heavy loops are likely responsible for the small-amplitude and large-amplitude current fluctuations.

The deletions in loops L3 and L4 increased $\Delta S^{\circ}_{O_3 \rightarrow O_2}$ (Table 1), indicating an increase in the the level of disorder of the local environment at the expense of the loss of intramolecular contacts in OccK1 ΔL3 and OccK1 ΔL4, but with no substantial changes in equilibrium energies. On the other hand, the variability of the effect of these deletions on transition and equilibrium enthalpies (Figure 6 and Table 1) suggests that alterations in one long extracellular loop (L3 or L4) not only remove native intramolecular contacts but also produce new interactions between the respective loop and other loops or among the other loops.[68] Because both deletions in L3 and L4 impacted the single-channel $O_1 \rightarrow O_2$, $O_2 \rightarrow O_1$, and $O_3 \rightarrow O_2$ current transitions, these findings confirm the high-resolution X-ray crystal structure of WT-OccK1 that reveals exposure of these large loops to the channel lumen.[22]

In summary, we examined the temperature dependence of the three-state discrete dynamics of the current gating fluctuations of OccK1, an outer membrane protein channel from *P. aeruginosa*. OccK1 exhibited enthalpy-driven, large-amplitude, and infrequent current transitions between the O_1 and O_2 open substates. The reversible $O_1 \rightarrow O_2$ fluctuations are accompanied by a drastic decrease in equilibrium entropy, rendering the channel system more ordered in the energetically most favorable O_2 open substate than in the O_1 open substate. Moreover, OccK1 displayed entropy-driven, small-amplitude, and highly frequent current transitions between the O_3 and O_2 open substates. The small equilibrium free energies demonstrate that these transitions were never far from the equilibrium, whereas the large enthalpic and entropic contributions suggest significant structural alterations within the channel lumen with small changes in temperature. We also revealed a change in the energetically most favorable open substate at the lowest examined temperature of 4 °C. This finding has significant implications for other membrane protein channels that operate differently under various temperature regimes. For example, reversal of the most probable substate was also observed with the vanilloid receptor (VR) channel.[64] At <42 °C, the VR channel showed a mostly closed substate, which was decorated by rare and short-lived openings. However, at >42 °C, VR exhibited a drastic increase in overall activity. On the basis of these findings, it may be feasible, with further experimentation and rational molecular design, to construct β-barrel protein nanopore-based devices with functional features that display thermally induced switches.

■ ASSOCIATED CONTENT

Supporting Information

(i) Physical features of the extracellular loops of the WT-OccK1 protein, (ii) titration experiments with potassium phosphate buffer, (iii) purification test of the OccK1 protein channel by an SDS−PAGE assay, (iv) temperature-dependent single-channel electrical recordings at a negative applied transmembrane potentials, (v) standard histograms of fitted current amplitudes of the single-channel events, (vi) typical all-points current amplitude histograms of WT-OccK1, (vii) semilog Eyring plot of the four kinetic rate constants of the WT-OccK1 protein channel acquired at a negative applied transmembrane potential, (viii) properties of loop-deletion OccK1 mutants, (ix) graphic representations of the loop-deletion OccK1 mutants, (x) single-channel electrical recordings with loop-deletion OccK1 mutants at room temperature, (xi) enthalpic contributions to the single-channel fluctuations of the WT-OccK1 protein and loop-deletion OccK1 mutants, and (xii) determination of the minimal transition entropies and maximal transition energies of the WT-OccK1 protein. This material is available free of charge via the Internet at http://pubs.acs.org.

■ AUTHOR INFORMATION

Corresponding Author

*Department of Physics, Syracuse University, 201 Physics Building, Syracuse, NY 13244-1130. Phone: (315) 443-8078. Fax: (315) 443-9103. E-mail: lmovilea@physics.syr.edu.

Funding

This paper is funded in part by grants from the National Science Foundation (DMR-1006332 to L.M.) and the National Institutes of Health (R01 GM088403 to L.M. and R01 GM085785 to B.v.d.B.).

Notes

The authors declare no competing financial interest.

■ ACKNOWLEDGMENTS

We thank colleagues in the Movileanu and van den Berg research groups, who provided technical assistance at various stages of this work. We also thank two anonymous reviewers for critical reading of the manuscript and constructive comments.

■ REFERENCES

(1) Wimley, W. C. (2003) The versatile β-barrel membrane protein. *Curr. Opin. Struct. Biol. 13*, 404−411.
(2) Bainbridge, G., Gokce, I., and Lakey, J. H. (1998) Voltage gating is a fundamental feature of porin and toxin β-barrel membrane channels. *FEBS Lett. 431*, 305−308.
(3) Robertson, K. M., and Tieleman, D. P. (2002) Molecular basis of voltage gating of OmpF porin. *Biochem. Cell Biol. 80*, 517−523.
(4) Phale, P. S., Schirmer, T., Prilipov, A., Lou, K. L., Hardmeyer, A., and Rosenbusch, J. P. (1997) Voltage gating of *Escherichia coli* porin channels: Role of the constriction loop. *Proc. Natl. Acad. Sci. U.S.A. 94*, 6741−6745.
(5) Bainbridge, G., Mobasheri, H., Armstrong, G. A., Lea, E. J. A., and Lakey, J. H. (1998) Voltage-gating of *Escherichia coli* porin: A cystine-scanning mutagenesis study of loop 3. *J. Mol. Biol. 275*, 171−176.
(6) Mapingire, O. S., Henderson, N. S., Duret, G., Thanassi, D. G., and Delcour, A. H. (2009) Modulating effects of the plug, helix, and N- and C-terminal domains on channel properties of the PapC usher. *J. Biol. Chem. 284*, 36324−36333.
(7) Mohammad, M. M., Howard, K. R., and Movileanu, L. (2011) Redesign of a plugged β-barrel membrane protein. *J. Biol. Chem. 286*, 8000−8013.
(8) Liu, N., Samartzidou, H., Lee, K. W., Briggs, J. M., and Delcour, A. H. (2000) Effects of pore mutations and permeant ion concentration on the spontaneous gating activity of OmpC porin. *Protein Eng. 13*, 491−500.
(9) Basle, A., Iyer, R., and Delcour, A. H. (2004) Subconductance states in OmpF gating. *Biochim. Biophys. Acta 1664*, 100−107.
(10) Wager, B., Basle, A., and Delcour, A. H. (2010) Disulfide bond tethering of extracellular loops does not affect the closure of OmpF porin at acidic pH. *Proteins 78*, 2886−2894.
(11) Mohammad, M. M., and Movileanu, L. (2010) Impact of distant charge reversals within a robust β-barrel protein pore. *J. Phys. Chem. B 114*, 8750−8759.
(12) Mari, S. A., Koster, S., Bippes, C. A., Yildiz, O., Kuhlbrandt, W., and Muller, D. J. (2010) pH-induced conformational change of the β-barrel-forming protein OmpG reconstituted into native *E. coli* lipids. *J. Mol. Biol. 396*, 610−616.
(13) Villinger, S., Briones, R., Giller, K., Zachariae, U., Lange, A., de Groot, B. L., Griesinger, C., Becker, S., and Zweckstetter, M. (2010) Functional dynamics in the voltage-dependent anion channel. *Proc. Natl. Acad. Sci. U.S.A. 107*, 22546−22551.
(14) Lepore, B. W., Indic, M., Pham, H., Hearn, E. M., Patel, D. R., and van den, B. B. (2011) Ligand-gated diffusion across the bacterial outer membrane. *Proc. Natl. Acad. Sci. U.S.A. 108*, 10121−10126.
(15) Bond, P. J., Derrick, J. P., and Sansom, M. S. (2007) Membrane simulations of OpcA: Gating in the loops? *Biophys. J. 92*, L23−L25.
(16) Luan, B., Caffrey, M., and Aksimentiev, A. (2007) Structure refinement of the OpcA adhesin using molecular dynamics. *Biophys. J. 93*, 3058−3069.
(17) Hong, H., Szabo, G., and Tamm, L. K. (2006) Electrostatic couplings in OmpA ion-channel gating suggest a mechanism for pore opening. *Nat. Chem. Biol. 2*, 627−635.
(18) Cheneke, B. R., van den Berg, B., and Movileanu, L. (2011) Analysis of gating transitions among the three major open states of the OpdK channel. *Biochemistry 50*, 4987−4997.
(19) Tamber, S., Ochs, M. M., and Hancock, R. E. (2006) Role of the novel OprD family of porins in nutrient uptake in *Pseudomonas aeruginosa*. *J. Bacteriol. 188*, 45−54.
(20) Hancock, R. E. W., and Tamber, S. (2004) Porins of the Outer Membrane of *Pseudomonas aeruginosa*. In *Bacterial and Eukaryotic Porins: Structure, Function, Mechanism* (Benz, R., Ed.) pp 61−77, Wiley-VCH, Weinheim, Germany.
(21) Biswas, S., Mohammad, M. M., Patel, D. R., Movileanu, L., and van den Berg, B. (2007) Structural insight into OprD substrate specificity. *Nat. Struct. Mol. Biol. 14*, 1108−1109.
(22) Eren, E., Vijayaraghavan, J., Liu, J., Cheneke, B. R., Touw, D. S., Lepore, B. W., Indic, M., Movileanu, L., and van den Berg, B. (2012) Substrate specificity within a family of outer membrane carboxylate channels. *PLoS Biol. 10*, e1001242.
(23) Liu, J., Eren, E., Vijayaraghavan, J., Cheneke, B. R., Indic, M., van den Berg, B., and Movileanu, L. (2012) OccK Channels from *Pseudomonas aeruginosa* Exhibit Diverse Single-channel Electrical Signatures, but Conserved Anion Selectivity. *Biochemistry 51*, 2319−2330.
(24) Biswas, S., Mohammad, M. M., Movileanu, L., and van den Berg, B. (2008) Crystal structure of the outer membrane protein OpdK from *Pseudomonas aeruginosa*. *Structure 16*, 1027−1035.
(25) Guzman, L. M., Belin, D., Carson, M. J., and Beckwith, J. (1995) Tight regulation, modulation, and high-level expression by vectors containing the arabinose PBAD promotor. *J. Bacteriol. 177*, 4121−4130.
(26) Mohammad, M. M., Prakash, S., Matouschek, A., and Movileanu, L. (2008) Controlling a single protein in a nanopore through electrostatic traps. *J. Am. Chem. Soc. 130*, 4081−4088.
(27) Colquhoun, D., and Sigworth, F. J. (1995) Fitting and statistical analysis of single-channel records. In *Single-channel recording* (Sackmann, B. N. E., Ed.) 2nd ed., pp 483−587, Plenum Press, New York.
(28) Mortensen, M., and Smart, T. G. (2007) Single-channel recording of ligand-gated ion channels. *Nat. Protoc. 2*, 2826−2841.
(29) McManus, O. B., Blatz, A. L., and Magleby, K. L. (1987) Sampling, Log Binning, Fitting, and Plotting Durations of Open and Shut Intervals From Single Channels and the Effects of Noise. *Pfluegers Arch. 410*, 530−553.
(30) McManus, O. B., and Magleby, K. L. (1988) Kinetic states and modes of single large-conductance calcium-activated potassium channels in cultured rat skeletal-muscle. *J. Physiol. (Oxford, U.K.) 402*, 79−120.
(31) Movileanu, L., Cheley, S., and Bayley, H. (2003) Partitioning of individual flexible polymers into a nanoscopic protein pore. *Biophys. J. 85*, 897−910.
(32) Jung, Y., Bayley, H., and Movileanu, L. (2006) Temperature-responsive protein pores. *J. Am. Chem. Soc. 128*, 15332−15340.
(33) Mohammad, M. M., and Movileanu, L. (2008) Excursion of a single polypeptide into a protein pore: Simple physics, but complicated biology. *Eur. Biophys. J. 37*, 913−925.
(34) Pettersen, E. F., Goddard, T. D., Huang, C. C., Couch, G. S., Greenblatt, D. M., Meng, E. C., and Ferrin, T. E. (2004) UCSF Chimera: A visualization system for exploratory research and analysis. *J. Comput. Chem. 25*, 1605−1612.
(35) Sackmann, B., and Neher, E. (1995) *Single-Channel Recording*, Kluwer Academic/Plenum Publishers, New York.
(36) Mohammad, M. M., and Movileanu, L. (2012) Protein Sensing with Engineered Protein Nanopores. In *Nanopore-Based Technology: Methods in Molecular Biology Series* (Graceva, M. E., Ed.) Vol. *870*, pp 21−37, Springer, New York.
(37) Stoll, V. S., and Blanchard, J. S. (1990) Buffers: Principles and practice. *Methods Enzymol. 182*, 24−38.
(38) Dawson, R. M. C., Elliot, D. C., Elliot, W. H., and Jones, K. M. (1986) *Data for biochemical research*, Clarendon Press, Oxford, U.K.
(39) Kang, X. F., Gu, L. Q., Cheley, S., and Bayley, H. (2005) Single Protein Pores Containing Molecular Adapters at High Temperatures. *Angew. Chem., Int. Ed. 44*, 1495−1499.
(40) Stoll, V. S., and Blanchard, J. S. (2009) Buffers: Principles and practice. *Methods Enzymol. 463*, 43−56.
(41) Aidley, D. J., and Stanfield, P. R. (1996) *Ion channels: Molecules in action*, Cambridge University Press, Cambridge, U.K.
(42) Urry, D. W., Venkatachalam, C. M., Spisni, A., Lauger, P., and Khaled, M. A. (1980) Rate theory calculation of gramicidin single-

channel currents using NMR-derived rate constants. *Proc. Natl. Acad. Sci. U.S.A. 77*, 2028−2032.
(43) Kostyuk, P. G., Shuba, Y., and Teslenko, V. I. (1989) Activation kinetics of single high-threshold calcium channels in the membrane of sensory neurons from mouse embryos. *J. Membr. Biol. 110*, 29−38.
(44) Moss, G. W. J., and Moczydlowski, E. (2002) Concepts of single-channel analysis: Inferring function from fluctuations. In *Ion Channels: A Practical Approach* (Ashley, R. H., Ed.) 2nd ed., pp 69−112, Oxford University Press, Oxford, U.K.
(45) Goodrich, C. P., Kirmizialtin, S., Huyghues-Despointes, B. M., Zhu, A. P., Scholtz, J. M., Makarov, D. E., and Movileanu, L. (2007) Single-molecule electrophoresis of β-hairpin peptides by electrical recordings and Langevin dynamics simulations. *J. Phys. Chem. B 111*, 3332−3335.
(46) Bikwemu, R., Wolfe, A. J., Xing, X., and Movileanu, L. (2010) Facilitated translocation of polypeptides through a single nanopore. *J. Phys.: Condens. Matter 22*, 454117.
(47) Hill, T. L. (1976) Diffusion frequency factors in some simple examples of transition-state rate theory. *Proc. Natl. Acad. Sci. U.S.A. 73*, 679−683.
(48) Jaikaran, D. C. J., and Woolley, G. A. (1995) Characterization of thermal-isomerization at the single-molecule level. *J. Phys. Chem. 99*, 13352−13355.
(49) Howorka, S., Movileanu, L., Braha, O., and Bayley, H. (2001) Kinetics of duplex formation for individual DNA strands within a single protein nanopore. *Proc. Natl. Acad. Sci. U.S.A. 98*, 12996−13001.
(50) Andersen, O. S. (1999) Graphic representation of the results of kinetic analyses. *J. Gen. Physiol. 114*, 589−590.
(51) Lauger, P. (1973) Ion transport through pores: A rate-theory analysis. *Biochim. Biophys. Acta 311*, 423−441.
(52) Jordan, P. C. (1999) Ion permeation and chemical kinetics. *J. Gen. Physiol. 114*, 601−603.
(53) Hille, B. (2001) *Ion Channels of Excitable Membranes*, Sinauer Associates, Inc., Sunderland, MA.
(54) Csanady, L., Nairn, A. C., and Gadsby, D. C. (2006) Thermodynamics of CFTR channel gating: A spreading conformational change initiates an irreversible gating cycle. *J. Gen. Physiol. 128*, 523−533.
(55) Nache, V., Kusch, J., Biskup, C., Schulz, E., Zimmer, T., Hagen, V., and Benndorf, K. (2008) Thermodynamics of activation gating in olfactory-type cyclic nucleotide-gated (CNGA2) channels. *Biophys. J. 95*, 2750−2758.
(56) Hanggi, P., Talkner, P., and Borkovec, M. (1990) Reaction-Rate Theory: 50 Years After Kramers. *Rev. Mod. Phys. 62*, 251−341.
(57) Oliveberg, M., Tan, Y. J., and Fersht, A. R. (1995) Negative activation enthalpies in the kinetics of protein folding. *Proc. Natl. Acad. Sci. U.S.A. 92*, 8926−8929.
(58) Movileanu, L., Benevides, J. M., and Thomas, G. J. (2002) Determination of base and backbone contributions to the thermodynamics of premelting and melting transitions in B DNA. *Nucleic Acids Res. 30*, 3767−3777.
(59) Gupta, S., and Auerbach, A. (2011) Mapping heat exchange in an allosteric protein. *Biophys. J. 100*, 904−911.
(60) Chimerel, C., Movileanu, L., Pezeshki, S., Winterhalter, M., and Kleinekathofer, U. (2008) Transport at the nanoscale: Temperature dependance of ion conductance. *Eur. Biophys. J. 38*, 121−125.
(61) Biro, I., Pezeshki, S., Weingart, H., Winterhalter, M., and Kleinekathofer, U. (2010) Comparing the temperature-dependent conductance of the two structurally similar *E. coli* porins OmpC and OmpF. *Biophys. J. 98*, 1830−1839.
(62) Marchal, S., Font, J., Ribo, M., Vilanova, M., Phillips, R. S., Lange, R., and Torrent, J. (2009) Asymmetric kinetics of protein structural changes. *Acc. Chem. Res. 42*, 778−787.
(63) Noronha, M., Gerbelova, H., Faria, T. Q., Lund, D. N., Smith, D. A., Santos, H., and Macanita, A. L. (2010) Thermal unfolding kinetics of ubiquitin in the microsecond-to-second time range probed by Tyr-59 fluorescence. *J. Phys. Chem. B 114*, 9912−9919.
(64) Liu, B., Hui, K., and Qin, F. (2003) Thermodynamics of heat activation of single capsaicin ion channels VR1. *Biophys. J. 85*, 2988−3006.
(65) Yao, J., Liu, B., and Qin, F. (2009) Rapid temperature jump by infrared diode laser irradiation for patch-clamp studies. *Biophys. J. 96*, 3611−3619.
(66) Gupta, S., and Auerbach, A. (2011) Temperature dependence of acetylcholine receptor channels activated by different agonists. *Biophys. J. 100*, 895−903.
(67) Dunitz, J. D. (1995) Win some, lose some: Enthalpy-entropy compensation in weak intermolecular interactions. *Chem. Biol. 2*, 709−712.
(68) Correa, A. M., Bezanilla, F., and Latorre, R. (1992) Gating kinetics of batrachotoxin-modified Na^+ channels in the squid giant axon. Voltage and temperature effects. *Biophys. J. 61*, 1332−1352.
(69) Wolfe, A. J., Mohammad, M. M., Cheley, S., Bayley, H., and Movileanu, L. (2007) Catalyzing the translocation of polypeptides through attractive interactions. *J. Am. Chem. Soc. 129*, 14034−14041.